the FEBS Journal

Competition between neighboring topogenic signals during membrane protein insertion into the ER

Magnus Monné*, Tara Hessa, Laura Thissen and Gunnar von Heijne

Department of Biochemistry and Biophysics, Stockholm University, Sweden

Keywords
endoplasmic reticulum; kinetics; membrane protein; positive inside rule; topology

Correspondence
G. von Heijne, Department of Biochemistry and Biophysics, Stockholm University, SE-106 91 Stockholm, Sweden
Fax: +46 8 153679
Tel: +46 8 162590
E-mail: gunnar@dbb.su.se

***Present address**
Medical Research Council, Dunn Human Nutrition Unit, Hills Road, Wellcome Trust/MRC Building, Cambridge CB2 2XY, UK

(Received 1 July 2004, revised 3 August 2004, accepted 11 August 2004)

doi:10.1111/j.1432-1033.2004.04394.x

To better define the mechanism of membrane protein insertion into the membrane of the endoplasmic reticulum, we measured the kinetics of translocation across microsomal membranes of the N-terminal lumenal tail and the lumenal domain following the second transmembrane segment (TM2) in the multispanning mouse protein Cig30. In the wild-type protein, the N-terminal tail translocates across the membrane before the downstream lumenal domain. Addition of positively charged residues to the N-terminal tail dramatically slows down its translocation and allows the downstream lumenal domain to translocate at the same time as or even before the N-tail. When TM2 is deleted, or when the loop between TM1 and TM2 is lengthened, addition of positively charged residues to the N-terminal tail causes TM1 to adopt an orientation with its N-terminal end in the cytoplasm. We suggest that the topology of the TM1-TM2 region of Cig30 depends on a competition between TM1 and TM2 such that the transmembrane segment that inserts first into the ER membrane determines the final topology.

The topology of integral membrane proteins is normally determined at the time of insertion into a target membrane. In both eukaryotic and prokaryotic cells, most membrane proteins are inserted initially into the endoplasmic reticulum (ER) or inner bacterial membranes by homologous translocation machineries: the Sec61p complex in eukaryotes and the SecYEG complex in prokaryotes [1,2]. Although the sequence determinants that control the final topology are fairly well understood [3,4], very little is known about the kinetics of the insertion process and whether this has any bearing on the topology. A widely accepted model is that insertion of successive transmembrane segments proceeds sequentially from the N- to the C-terminus [5,6], but detailed studies on the topology adopted by various engineered model proteins have suggested the possibility of nonsequential insertion mechanisms, where interactions between neighboring transmembrane segments or re-orientation of transmembrane segments during the insertion process determine the final topology [7–12].

Using the modification kinetics of engineered glycosylation sites as a measure of translocation rate, we now show that the rate of translocation of an N-terminal lumenal tail is influenced strongly by the presence of charged amino acids in the tail, and that the size of the loop separating two transmembrane segments can affect the final topology adopted by the protein. There is a strong correlation between the timing of the translocation of the N-tail relative to a downstream lumenal domain and the final topology adopted by the protein, suggesting that different parts of the protein with different topological preferences may compete within the translocon.

Abbreviations
OST, oligosaccharide transferase enzyme; TM, transmembrane segment; RM, rough microsomes.

Results

Translocation of lumenal domains in Cig30 N-tail Arg mutants

In a previous study [8], we showed that efficient translocation across the ER membrane of a mutated form of the polytopic murine Cig30 protein (four Arg residues added to the 35-residues long lumenal N-tail) [13] requires the presence of at least two of the five predicted transmembrane segments, strongly suggesting that membrane insertion may not always be strictly N-to-C-terminal. Similar results were also obtained with ProW, another multispanning membrane protein with a translocated N-tail [7].

In order to directly characterize the timing of translocation of different lumenal parts of Cig30, we engineered constructs where a region containing the two most N-terminal transmembrane segments (residues 1–100) from Cig30 and Cig30(4R), a mutant with four Args added between positions 9 and 10 in the N-tail [8], is fused to the P2 reporter domain from the *Escherichia coli* Lep protein, Fig. 1A. The insertion of the constructs into dog pancreas rough microsomes (RMs) was followed in an *in vitro* translation/translocation system by determining the kinetics of glycosylation of acceptor sites with the Asn located either in position 6 in the N-tail (G1 site, Asn-Phe-Ser), in position 118 the P2 domain (G2 site, Asn-Ser-Thr), or in both. The kinetic assay is based on the fact that N-linked glycosylation can only be performed by the lumenally oriented oligosaccharide transferase enzyme (OST) in intact microsomes and not when the microsomes have been dissolved by detergent. The transla-

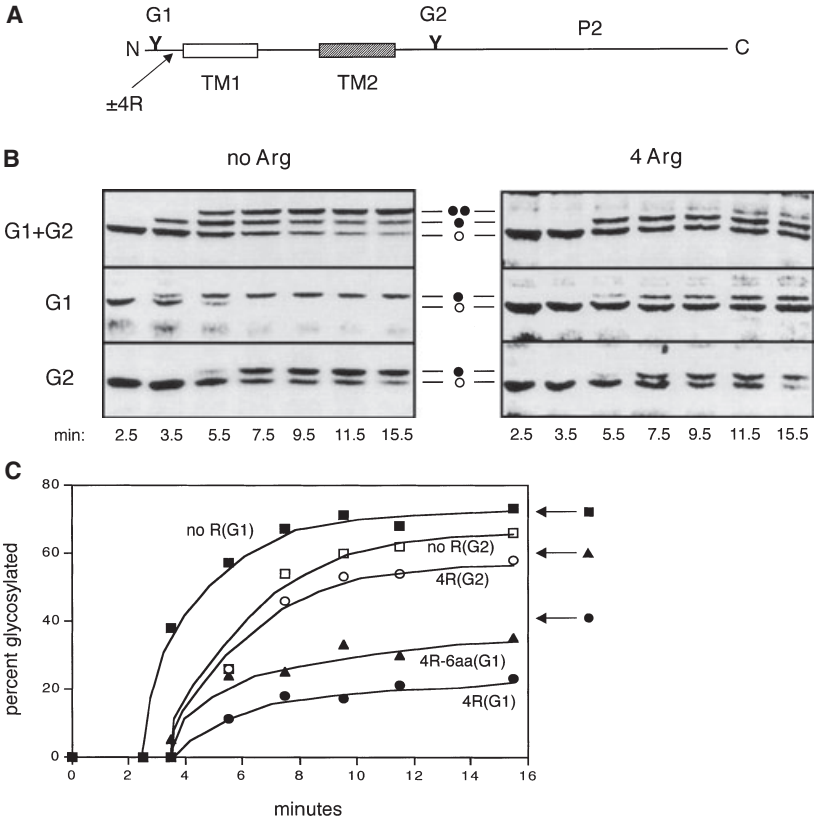

Fig. 1. Initiation of N-tail translocation is delayed in Cig30(1–100)(4R)-P2. (A) Schematic representation of the Cig30(1–100)(wt)-P2 and Cig30(1–100)(4R)-P2 constructs. G1 and G2 indicate acceptor sites for N-linked glycosylation. (B) *In vitro* translation of mRNAs encoding Cig30(1–100)(wt)-P2 (left) and Cig30(1–100)(4R)-P2 (right) constructs carrying both the G1 and G2 glycosylation acceptor sites (top), only the G1 site (middle), or only the G2 site (bottom). The translation initiation inhibitor aurintricarboxylic acid was added to the translation mix 1.5 min after addition of the mRNA, and Triton X-100 was then added at the indicated times. The total translation time was 60 min. ○, Unglycosylated molecules; ●, singly glycosylated molecules; ●●, doubly glycosylated molecules. (C) Quantification of the data for Cig30(1–100)(wt)-P2 and Cig30(1–100)(4R)-P2 constructs carrying either the G1 or the G2 glycosylation acceptor site (middle and bottom panels in Fig. 1B). ■, Cig30(1–100)(wt)-P2 (G1); □, Cig30(1–100)(wt)-P2 (G2); ●, Cig30(1–100)(4R)-P2 (G1); ○, Cig30(1–100)(4R)-P2 (G2); ▲, Cig30(1–100)(4R-6aa)-P2 (G1). The final glycosylation levels after a 60 min incubation are shown by arrows for Cig30(1–100)(wt)-P2 (G1), Cig30(1–100)(4R)-P2 (G1), and Cig30(1–100)(4R-6aa)-P2 (G1). The maximum level of glycosylation obtained in the *in vitro* system is around 80%.

tion reaction, in contrast, is insensitive to the presence of detergent, and the glycosylation status of nascent polypeptide chains can thus be determined as a function of translation time by adding detergent at different times after chain initiation and then allowing translation to proceed to completion [14,15].

As seen in Fig. 1B (left panel), for Cig30(1–100)(wt)-P2, the G1 acceptor site in the N-tail is glycosylated more rapidly than the G2 acceptor site in the P2 domain. For the G2 site to become glycosylated, an additional 65 residues beyond this site must be polymerized to bridge the distance between the OST active site and the ribosomal P-site [16], corresponding to a total chain length of 183 residues. From Fig. 1C, the $t_{1/2}$ for glycosylation of G2 is 6 min, corresponding to a translation rate of $183/360 = 0.5$ residues·s^{-1}, comparable to previously published values [14,15,17]. As an independent measure of the average translation rate, we also determined the $t_{1/2}$ necessary for the appearance of a 190-residues long, truncated form of Cig30 in the translation reaction to be 5.5 min, corresponding to an average translation rate of 0.6 residues·s^{-1} (data not shown).

Assuming that TM1 (residues 34–56) has to emerge from the ribosome before the protein can be targeted to the translocon, and given that the nascent-chain conducting tunnel in the ribosome covers some 30–40 residues of the nascent chain, the calculated $t_{1/2}$ for glycosylation of the G1 site in the N-tail is $90/0.5 =$ 180 s, in good agreement with the observed kinetics, Fig. 1C. We conclude that glycosylation of the G1 and G2 sites happen as soon as they become exposed to the lumen of the microsome, and that the kinetics of glycosylation is a good measure of the timing of translocation of the corresponding segment of the protein.

Compared to Cig30(1–100)(wt)-P2, the behavior of the Cig30(1–100)(4R)-P2 construct is strikingly different, Fig. 1B (right panel). The G2 site is glycosylated with indistinguishable kinetics compared to Cig30(1–100)(wt)-P2, while the modification of the G1 site is now dramatically delayed and is initiated concomitantly with or even after the modification of the G2 site in the P2 domain, Fig. 1C. It is also noteworthy that there is an initial, fast phase of glycosylation of the G1 site (up to a level of $\approx$20% glycosylation) followed by a much slower until the final level of 42% is reached (arrows). A similar slow phase has been seen recently for glycosylation of Asn-X-Thr acceptor sites located close to a protein's C-terminus [17]. A possible explanation could be that N-tails are so rapidly translocated across the membrane that some chains pass OST too fast to be glycosylated and only become modified in a slower, post-translational process.

The final level of glycosylation of the G1 site in Cig30(1–100)(4R)-P2 is lower than in Cig30(1–100)(wt)-P2 (42% vs. 69%); however, this seems to be due mainly to a partial blocking of the Asn-Phe-Ser acceptor site by the nearby Arg residues, as the addition of a six residues long spacer (VGAGVG) between the G1 site and the four Arg residues [construct Cig30(1–100)(4R-6aa)-P2] leads to an increase in the final glycosylation level to 60% without appreciably affecting the kinetics of the modification of the G1 site (Fig. 1C and data not shown). A similar increase in glycosylation efficiency (from 53% to 69%) was seen previously when the 4R insertion was moved from position 9 to position 28 in the N-tail of full-length Cig30(4R) [8], again consistent with a partial blocking effect of the 4R mutation when present next to the G1 glycosylation site.

We also followed the kinetics of glycosylation of the G1 site for the full-length Cig30 protein fused to the P2 reporter domain, and for a series of mutants with increasing numbers of Arg residues in the N-tail (Fig. 2). The initial delay increases with the number of Arg residues in the N-tail. The kinetics of modification of the G1 site in Cig30(wt)-P2 and Cig30(4R)-P2 are indistinguishable from the corresponding kinetics for the Cig30(1–100)(wt)-P2 and Cig30(1–100)(4R)-P2 constructs, respectively. Again, the glycosylation of the G1 site in the 4R and 5R mutants proceeds through a rapid phase up to $\approx$30% glycosylation followed by a much slower phase leading to a final level of 53%

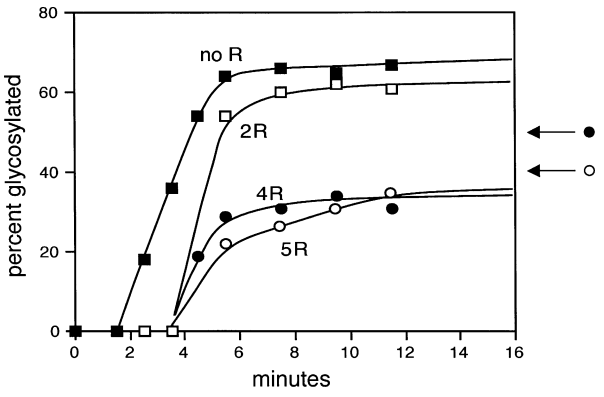

Fig. 2. Initiation of N-tail translocation is progressively delayed in Cig30(wt)-P2 when increasing number of Arg residues is added to the N-tail. Experiments were performed and quantified as in as in Fig. 1B, but using the Cig30(wt)-P2 fusion protein with 0, 2, 4, and five Arg residues added between residues 9 and 10 in the N-tail as indicated. Only the G1 glycosylation acceptor site in the N-tail is present in these constructs. ■, Cig30(wt)-P2 (G1); □, Cig30(2R)-P2 (G1); ●, Cig30(4R)-P2 (G1); ○, Cig30(5R)-P2 (G1). The final glycosylation levels after a 60 min incubation is shown by arrows for Cig30(4R)-P2 (G1) and Cig30(5R)-P2 (G1).

glycosylation for Cig30(4R)-P2 (63% when the six residues long spacer mentioned above is inserted into the N-tail) and to 39% for Cig30(5R)-P2.

We conclude that there is an initial delay in N-tail translocation, as measured by glycosylation of the G1 site, in both truncated and full-length Cig30 mutants with extra Arg residues in the N-tail compared to the wild-type protein, and that translocation of the lumenal P2 domain following the second transmembrane segment in the Cig30(1–100)(4R)-P2 construct, as measured by glycosylation of the G2 site, is initiated concomitant with or even before N-tail translocation.

Asp residues in the N-tail have a minor kinetic effect on translocation

We also tested the effect of placing four Asp residues in the Cig30 N-tail, both in the context of the full-length Cig30(wt)-P2 fusion and in Cig30(1–100)(wt)-P2. The G1 site in the N-tail of Cig30(4D)-P2 is glycosylated with slightly delayed kinetics compared to Cig30-P2, and the final level of glycosylation is the same for both constructs ($\approx$ 75%) (Fig. 3). A slight delay was also seen for Cig30(1–100)(4D)-P2. Thus, the 4D mutation has a weaker but still detectable effect on the translocation kinetics of the N-tail.

Competition between neighboring transmembrane segments

The delayed glycosylation of the G1 site in Cig30(1–100)(4R)-P2 suggested to us that the intrinsic topological preference of the N-tail/TM1 region in this construct may be N_{cyt}–C_{lum}, but that TM1 is either prevented from inserting with this orientation by the more rapid membrane insertion and translocation of the neighboring TM2/P2 domain, or that it initially inserts in the N_{cyt}–C_{lum} orientation but then re-orients as a result of the insertion of the TM2/P2 domain [9,11,18].

To gain further insight into this phenomenon, we compared two constructs where only the N-tail/TM1 region of Cig30 (residues 1–70) is fused to the P2 domain: one with the wild-type N-tail [Cig30(1–70)(wt)-P2], and one with the 4R mutation in the N-tail (Cig30(1–70)(4R)-P2), Fig. 4A. As shown previously [8], the G1 site in Cig30(1–70)(wt)-P2 was efficiently glycosylated, and only the G2 site in Cig30(1–70)(4R)-P2 was glycosylated to a final level of 74% (data not shown), indicating that the Cig30(1–70)(4R)-P2 is oriented with the opposite topology compared to the corresponding wt construct. The glycosylation kinetics of the G1 site in Cig30(1–70)-P2 and the G2 site in Cig30(1–70)(4R)-P2 were as expected from the positions of the respective glycosylation sites and the average translation rate (0.5 residues·s^{-1}), Fig. 4B.

We also tested the related construct Cig30(1–70)(4D)-P2 with four Asp residues in the N-tail. As noted above, glycosylation of the N-tail is somewhat delayed

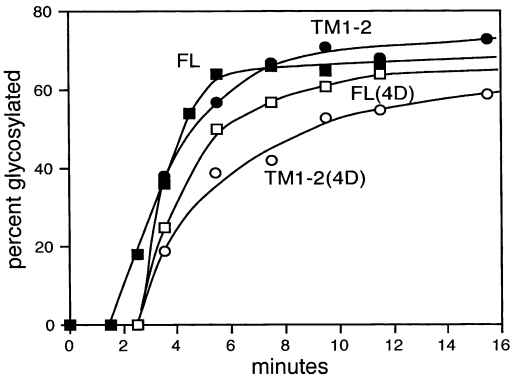

Fig. 3. Asp residues in the N-tail have a minor kinetic effect on translocation. Experiments were performed and quantified as in as in Fig. 1B, but using the Cig30(wt)-P2 (denoted FL) and Cig30(1–100)(wt)-P2 (denoted TM1-2) fusion proteins with or without four Asp residues added between residues 9 and 10 in the N-tail as indicated. Only the G1 glycosylation acceptor site in the N-tail is present in these constructs. ■, Cig30(wt)-P2 (G1); □, Cig30(4D)-P2 (G1); ●, Cig30(1–100)(wt)-P2 (G1); ○, Cig30(1–100)(4D)-P2 (G1).

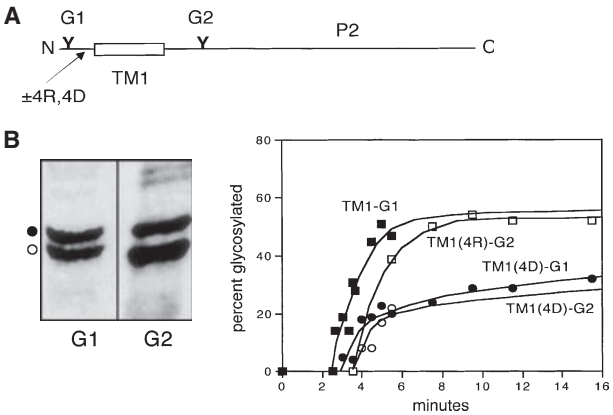

Fig. 4. Arg and Asp residues in the N-tail of the Cig30(1–70)(4R)-P2 construct promote the N_{cyt} orientation. (A) Schematic representation of the Cig30(1–70)-P2 constructs. (B) Experiments were performed and quantified as in as in Fig. 1B but using the Cig30(1–70)-P2 fusion protein (denoted TM1) with or without four Arg or four Asp residues added between residues 9 and 10 in the N-tail as indicated. Results for constructs containing either the G1 or the G2 glycosylation acceptor sites are shown. ■, Cig30(1–70)(wt)-P2 (G1); □, Cig30(1–70)(4R)-P2 (G2); ●, Cig30(1–70)(4D)-P2 (G1); ○, Cig30(1–70)(4D)-P2 (G2). *In vitro* translations of Cig30(1–70)(4D)-P2 constructs carrying either the G1 site in the N-tail or the G2 site in the P2 domain are also shown (left). ○, Unglycosylated molecules; ●, glycosylated molecules.

in the longer Cig30(1–100)(4D)-P2 and Cig30(4D)-P2 constructs compared to Cig30(1–100)(wt)-P2 and Cig30(wt)-P2. Interestingly, the 4D mutation has a clear effect on the topology of Cig30(1–70)(4D)-P2. This construct is glycosylated with about equal efficiencies on the G1 and G2 sites, Fig. 4B, and hence has a mixed topology with only about half the molecules in the N_{lum}–C_{cyt} orientation. Glycosylation of the N-tail is delayed in Cig30(1–70)(4D)-P2 compared to Cig30(1–70)(wt)-P2, and the G1 site is glycosylated only slightly before the G2 site in this construct (Fig. 4B).

The finding that TM1 adopts the N_{cyt}–C_{lum} orientation in Cig30(1–70)(4R)-P2 but the N_{lum}–C_{cyt} orientation in Cig30(1–100)(4R)-P2 indicated that the length of the loop between TM1 and TM2 may be a critical topological determinant, such that a longer loop might allow the intrinsic topological preference of the N-tail/TM1 region to become more dominant. We therefore made a series of constructs based on full-length Cig30(4R)-P2 where the length of the loop between TM1 and TM2 was increased from 11 to 72 residues (Fig. 5). Consistent with our expectations, the level of N-tail glycosylation decreased from 53% for the shortest loop to background levels (8%) for the longest loop. In the latter construct, when a glycosylation acceptor site was inserted in the TM1-TM2 loop it was efficiently modified (71% glycosylation; black circle, Fig. 5), showing that TM1 indeed has a N_{cy}–C_{lum} orientation in this case.

We conclude that the Cig30(4R) N-tail/TM1 region intrinsically prefers the N_{cyt}–C_{lum} orientation, and suggest that the translocation of the downstream segment is initiated very soon after the TM1 segment enters the translocon when TM2 is absent or when the separation between TM1 and TM2 is sufficiently long. When the TM1-TM2 loop is short, however, TM1 adopts its less preferred N_{lum}–C_{cyt} orientation.

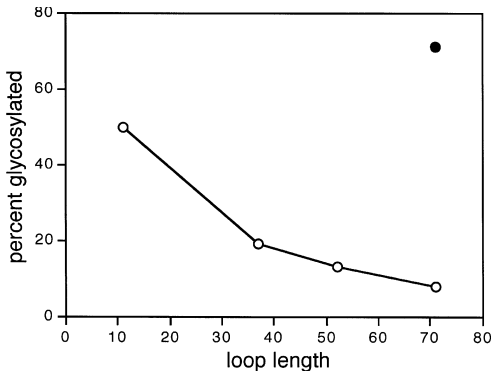

Fig. 5. Increased separation between TM1 and TM2 in Cig30(4R)-P2 favors a cytoplasmic location of the N-tail. Cig30(4R)-P2-derived constructs with increasingly long loops between TM1 and TM2 were translated in the presence of microsomes. ○, Percentage of molecules glycosylated on the G1 site in the N-tail; ● level of glycosylation of a glycosylation acceptor site engineered into in the loop between TM1 and TM2 in the construct with a 72 residues long loop.

For Cig30(1–70)(4D)-P2, the N_{lum}–C_{cyt} and N_{cyt}–C_{lum} orientations are roughly equally preferred, and the G1 and G2 sites are modified with similar kinetics. In Cig30(1–100)(4D)-P2 and Cig30(4D)-P2, in contrast, the N-tail is efficiently translocated in essentially 100% of the molecules.

Discussion

So far, not much is known about the kinetics of membrane protein insertion into the ER membrane and whether membrane protein topology is in some sense under kinetic control. Studies *in vivo* using an engineered phosphorylation site as a reporter for the translocation of an N-tail across the ER membrane have shown that targeting to the ER is rapid, and that the factors determining the overall rate of N-tail translocation are the time it takes for the ER targeting signal to become exposed outside the ribosome and the rate of the ensuing N-tail translocation reaction, which has been estimated to be $\approx$1.6 times faster than the translation rate on a per-residue basis [19]. A study using engineered glycosylation sites has further shown that N-tails are translocated in a C-to-N-terminal direction, starting from the N-terminal transmembrane segment [7]. Finally, the extracytoplasmic segments in the multispanning membrane protein bacterioopsin have been shown to become exposed on the extracellular surface cotranslationally and in a sequential order starting with the N-tail when the protein is expressed in *Halobacterium salinarium* [6]. Neighboring transmembrane segments may also affect each other's orientation, suggesting a rather complex process of topology determination in the ER translocon [7–9,11,20].

Here, we have used engineered glycosylation sites in fusions between the full-length mouse Cig30 protein, the Cig30 N-tail/TM1 region (residues 1–70), and the N-tail/TM1/TM2 region (residues 1–100) and a reporter domain (P2) from the *E. coli* Lep protein to follow the translocation of the N-tail and the P2 domain across microsomal membranes *in vitro*. As estimated from the average translation rate in the *in vitro* system, the engineered glycosylation sites become modified as soon as they enter the ER lumen. The glycosylation kinetics of a given acceptor site can thus be used to track the translocation of the corresponding domain in the model protein.

For Cig30(1–100)(wt)-P2, we find a sequential translocation process where the N-tail is translocated as

soon as TM1 enters the translocon, followed by translocation of the P2 domain initiated by TM2, Fig. 1.

In sharp contrast, however, the kinetics of N-tail translocation is strongly delayed in the Cig30(1–100)(4R)-P2 mutant (where four Arg residues have been introduced into the N-tail), and is initiated at about the same time or even after translocation of the P2 domain (Fig. 1). Similarly, addition of two to five Arg residues to the N-tail of the full-length Cig30-P2 fusion progressively delays the onset of N-tail translocation (Fig. 2). Interestingly, addition of four Asp residues to the N-tail of full-length Cig30(wt)-P2 and to Cig30(1–100)-P2 also causes a somewhat delayed onset of translocation (Fig. 3).

The delayed translocation of the N-tail in Cig30(4R)-P2 and Cig30(1–100)(4R)-P2 suggests that the N-tail/TM1 region in these constructs has an intrinsic preference for inserting into the ER with N_{cyt}–C_{lum} orientation – in keeping with the so-called positive-inside rule [21] – rather than the N_{lum}–C_{cyt} orientation adopted in the presence of TM2. This is indeed the case. When the Cig30(4R) N-tail/TM1 region is fused directly to the P2 reporter domain [construct Cig30(1–70)(4R)-P2], P2 is translocated rapidly across the ER membrane (Fig. 4). In contrast, the N-tail is translocated rapidly in Cig30(1–70)(wt)-P2. Finally, Cig30(1–70)(4D)-P2 adopts a mixed topology with roughly equal amounts of N_{cyt}–C_{lum} and N_{lum}–C_{cyt} oriented molecules, and with almost identical translocation kinetics for the N-tail and the P2 domain. For constructs such as Cig30(1–100)(4R)-P2 where the N-tail/TM1 region has an intrinsic preference for the N_{cyt}–C_{lum} orientation, more of the N_{cyt}–C_{lum} orientation is observed when the loop between TM1 and TM2 is progressively lengthened (Fig. 5).

These results show a strong correlation between the relative timing of translocation initiated from the TM1 and TM2 transmembrane segments and the final topology of the protein, suggesting that some topological signals may dominate over others within the translocon. A possible mechanism of topology formation suggested by these results, Fig. 6, is that TM1 enters the translocon first and thus gets a head start over TM2. If the N-tail is not highly charged, it translocates rapidly, fixing TM1 in a N_{lum}–C_{cyt} orientation. TM2 then initiates translocation of the P2 domain. In contrast, if the N-tail contains a sufficient number of positively charged residues it prefers a N_{cyt}–C_{lum} orientation. This is the orientation obtained when only TM1 is present, or when the connecting loop between TM1 and TM2 is sufficiently long. If the connecting loop is short, however, either of two things may happen: (a) TM1 inserts initially in its preferred N_{cyt}–C_{lum} orientation but is then somehow forced to re-orient to the N_{lum}–C_{cyt} orientation when TM2 inserts [9,11], or (b) TM1 does not have time to insert before TM2 initiates rapid translocation of the P2 domain, giving TM1 no option but to translocate the N-tail. A somewhat more complicated variation on (a), suggested by some recent work [9,18], is that TM1 inserts initially in the N_{lum}–C_{cyt} orientation, but then re-orients (before it has time to become glycosylated) if the N-tail contains many charged residues, unless the rapid insertion of TM2 prevents re-orientation.

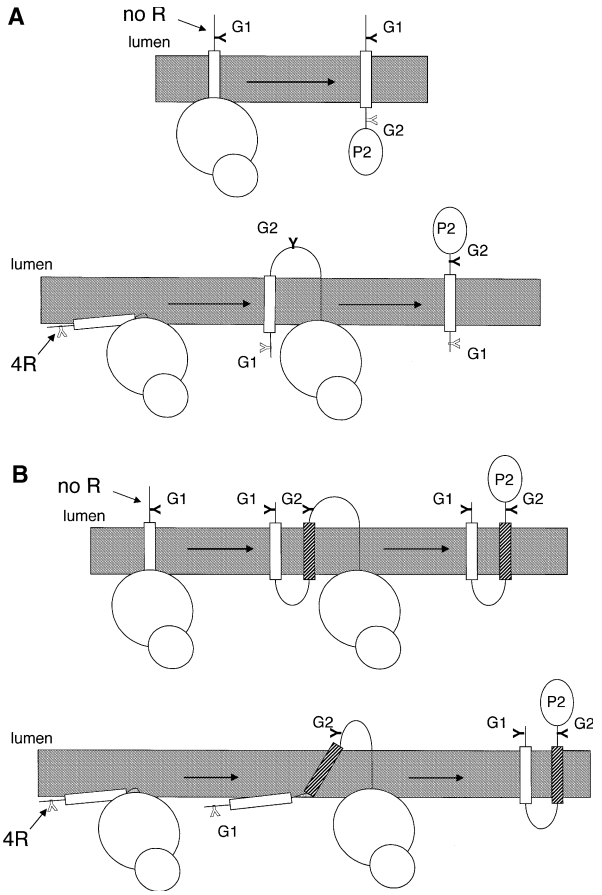

Fig. 6. Model for the membrane insertion of Cig30(1–70)-P2 (panel A) and Cig30(1–100)-P2 (panel B) derived constructs into the microsomal membrane. The top cartoon in each panel shows constructs such as Cig30(1–100)(wt)-P2 that have no additional charge residues in their N-tail, while the bottom cartoons are for constructs such as Cig30(1–100)(4R)-P2 with a positively charged N-tail. TM1 is white and TM2 is striped. The G1 and G2 glycosylation acceptor sites are indicated; unfilled symbols represent nonglycosylated sites, filled symbols represent glycosylated sites.

Regardless of the exact mechanism, however, our results strongly suggest that there is a critical period from about the time when TM1 enters the translocon during which the appearance of TM2 in the translocon

can affect the final orientation of TM1. One attractive possibility is that the end of this critical period corresponds to the point where TM1 exits the translocation channel and becomes lodged in the surrounding lipid bilayer [22–24].

In summary, we have shown that the introduction of charged residues in the lumenal N-tail of Cig30 causes a strong delay in the translocation of the N-tail that goes in parallel with an increased intrinsic preference for a N_{cyt}–C_{lum} orientation of the isolated N-tail/TM1 domain. This intrinsic preference can be overridden by the following TM2 segment (that also has a preference for the N_{cyt}–C_{lum} orientation), provided that the loop between TM1 and TM2 is short. The final topology of the protein thus seems to result from a finely tuned competition between neighboring topogenic signals (the TM segments and their immediate flanking regions) that is influenced both by the presence or absence of charged residues (where positively charged residues are more potent topological determinants than negatively charged ones), possibly by the hydrophobicity of the transmembrane segments [25], and by the length of the loops separating them [9]. Finally, our results suggest that the 'positive inside' rule for membrane protein topology [21] may at least in part be explained by a reduction in the rate of membrane translocation of segments of the nascent polypeptide chain with a high content of positively charged residues.

Experimental procedures

Enzymes and chemicals

Unless otherwise stated, all enzymes were from Promega (Madison, WI, USA). Ribonucleotides, deoxyribonucleotides, dideoxyribonucleotides, the cap analog m7G(5′)ppp(5′)G, T7 DNA polymerase, and [^{35}S]methionine were from Amersham–Pharmacia Biotech (Uppsala, Sweden). Plasmid pGEM1, dithiothreitol, BSA, RNasin and rabbit reticulocyte lysate were from Promega (Madison). Spermidine, aurintricarboxylic acid, and Triton X-100 were from Sigma–Aldrich Inc. (St. Louis, MO, USA). Oligonucleotides were from Cybergene (Stockholm, Sweden).

DNA techniques

*Sal*I and *Xba*I restriction sites were introduced by PCR at the 5′ and 3′ ends of the *cig30* gene, respectively. The PCR fragment was cloned into phage M13mp18, and into a pGEM1-derived plasmid after a modified upstream region of the *lepB* gene containing a Kozak consensus sequence [26] for efficient ribosome binding. Site-directed mutagenesis was performed according to Kunkel [27,28] to introduce four Arg codons between the 9th and 10th codon in the *cig30* coding region. In some constructs, the natural G1 glycosylation site of Cig30 was silenced by mutating Asn6→Thr, and in others a six residue spacer (VGAGVG) was inserted after the 9th codon using the QuickChange kit (Stratagene).

Cig30 fusions with the P2 domain of Lep were made by introducing a *Nde*I site in codon 70 (i.e. before TM2) or in codon 100 (after TM2) by PCR amplification using primers encoding the two flanking restriction sites. The *Sal*I-*Nde*I restricted PCR fragments were cloned into a pGEM1-derived vector containing the P2 domain (codons 81–323) of Lep preceded by a *Nde*I site. The natural glycosylation site in P2 was silenced by mutating Asn214 → Gln and two version of P2, with and without the G2 consensus glycosylation site [NST(96–98)], were used.

For the elongation of the loop between TM1 and TM2, parts of the P2 domain of Lep were cloned into the first cytoplasmic loop in Cig30 utilizing engineered *Eco*RV and *Nde*I restriction sites. The 11 residues in the Cig30 TM1–TM2 loop were retained both in the N- and C-terminal parts of the elongated loops. In one construct, an Asn-Ser-Thr glycosylation acceptor site was introduced in the middle of the 72 residues long loop. The three resulting loops had the following lengths and sequences (Lep-derived segments are underlined; the three residues LIG in the 72 residues long loop that were exchanged to NST in the glycosylation mutant are in bold; numbers refer to residue positions in the Cig30 and Lep proteins): 40 residues, QRP(67)Y(81)EPFQIPSGSMMPTLLI(97)DI R(57)trk; 55 residues, QRP(67)Y(81)EPFQIPSGSMMPTLLIGDFILVEKFAYGIKD(112)DIR(57)trk; 72 residues, QRP(67)Y(81)EPFQIPSGSMMPTL**LIG**DFILVEKFAYGIKDPIYQKTLIENGHPKRG(128)DIR(57)TRK.

All constructs were confirmed by sequencing of plasmid DNA using T7 DNA polymerase.

In vitro expression

Constructs in pGEM1 were amplified using a 5′ primer hybridizing upstream of the SP6 promoter and the 3′ primers described above. The PCR products were transcribed by SP6 RNA polymerase for 1 h at 37 °C. The transcription mixture was as follows: 1–5 μg DNA template, 5 μL 10× SP6 H-buffer [400 mM Hepes/KOH (pH 7.4), 60 mM Mg acetate, 20 mM spermidine/HCl], 5 μL BSA (1 mg·mL^{-1}), 5 μL m7G(5′)ppp(5′)G (10 mM), 5 μL dithiothreitol (50 mM), 5 μL rNTP mix (10 mM ATP, 10 mM CTP, 10 mM UTP, 5 mM GTP), 18.5 μL H_2O, 1.5 μL RNase inhibitor (50 units), 0.5 μL SP6 RNA polymerase (20 units).

Translation of 1 μL mRNA in 9 μL nuclease-treated reticulocyte lysate, 1 μL RNase inhibitor (40 units·μL^{-1}), 1 μL [^{35}S]Met (10 μCi·μL^{-1}), 1 μL amino acids mix (1 mM of each amino acid except Met), 1 μL dog pancreas rough

microsomes was performed as described [29] at 30 °C for 60 min.

For the kinetic studies, the translation mix was preincubated 4 min before [^{35}S]Met and mRNA was added, and the translation initiation inhibitor aurintricarboxylic acid was added to a final concentration of 0.075 mM after an additional 1.5 min [14]. Samples were removed at different time points and were incubated further at 30 °C in the presence of 1% (v/v) Triton X-100 until a total translation time of 60 min.

Translation products were analyzed by SDS/PAGE and gels were quantified on a Fuji FLA-3000 phosphorimager using the IMAGE READER 8.1j software. The glycosylation efficiency was calculated as the quotient between the intensity of the glycosylated band divided by the summed intensities of the glycosylated and nonglycosylated bands. In general, the glycosylation efficiency varied by no more than ±5% between different experiments (at least two independent measurements were made for all constructs).

Acknowledgements

This work was supported by grants from the Swedish Cancer Foundation and the Swedish Research Council to G.vH. Dog pancreas microsomes were a kind gift from Dr M. Sakaguchi, University of Hyogo, Japan.

References

1 Johnson AE & van Waes MA (1999) The translocon: a dynamic gateway at the ER membrane. *Annu Rev Cell Dev Biol* **15**, 799–842.
2 de Gier JW & Luirink J (2001) Biogenesis of inner membrane proteins in *Escherichia coli*. *Mol Microbiol* **40**, 314–322.
3 Goder V & Spiess M (2001) Topogenesis of membrane proteins: determinants and dynamics. *FEBS Lett* **504**, 87–93.
4 von Heijne G (2000) Recent advances in the understanding of membrane protein assembly and structure. *Quart Rev Biophys* **32**, 285–307.
5 Blobel G (1980) Intracellular protein topogenesis. *Proc Natl Acad Sci USA* **77**, 1496–1500.
6 Dale H, Angevine CM & Krebs MP (2000) Ordered membrane insertion of an archaeal opsin *in vivo*. *Proc Natl Acad Sci USA* **97**, 7847–7852.
7 Nilsson I, Witt S, Kiefer H, Mingarro I & von Heijne G (2000) Distant downstream sequence determinants can control N-tail translocation during protein insertion into the endoplasmic reticulum membrane. *J Biol Chem* **275**, 6207–6213.
8 Monné M, Gafvelin G, Nilsson R. & von Heijne G (1999) N-tail translocation in a eukaryotic polytopic membrane protein – Synergy between neighboring transmembrane segments. *Eur J Biochem* **263**, 264–269.
9 Goder V, Bieri C & Spiess M (1999) Glycosylation can influence topogenesis of membrane proteins and reveals dynamic reorientation of nascent polypeptides within the translocon. *J Cell Biol* **147**, 257–266.
10 Anthony V & Skach WR (2002) Molecular mechanism of P-glycoprotein assembly into cellular membranes. *Curr Protein Pept Sci* **3**, 485–501.
11 Lu Y, Turnbull IR, Bragin A, Carveth K, Verkman AS & Skach WR (2000) Reorientation of aquaporin-1 topology during maturation in the endoplasmic reticulum. *Mol Biol Cell* **11**, 2973–2985.
12 Carveth K, Buck T, Anthony V & Skach WR (2002) Cooperativity and flexibility of cystic fibrosis transmembrane conductance regulator transmembrane segments participate in membrane localization of a charged residue. *J Biol Chem* **277**, 39507–39514.
13 Tvrdik P, Asadi A, Kozak L, Nedergaard J, Cannon B & Jacobsson A (1997) Cig30, a mouse member of a novel membrane protein gene family is involved in the recruitement of brown adipose tissue. *J Biol Chem* **272**, 31738–31746.
14 Garoff H, Huylebroeck D, Robinson A, Tillman U, Liljeström & P (1990) The signal sequence of the p62-protein of Semliki Forest virus is involved in initiation but not in completing chain translocation. *J Cell Biol* **111**, 867–876.
15 Rothman J & Lodish H (1977) Synchronised transmembrane insertion and glycosylation of a nascent membrane protein. *Nature* **269**, 775–780.
16 Whitley P, Nilsson IM & von Heijne G (1996) A nascent secretory protein may traverse the ribosome/ER translocase complex as an extended chain. *J Biol Chem* **271**, 6241–6244.
17 Hessa T, Monné, M & von Heijne G (2003) Stop-transfer efficiency of marginally hydrophobic stop-transfer segments depends on the length of the C-terminal tail. *EMBO Report* **4**, 178–183.
18 Goder V & Spiess M (2003) Molecular mechanism of signal sequence orientation in the endoplasmic reticulum. *EMBO J* **22**, 3645–3653.
19 Goder V, Crottet P & Spiess M (2000) *In vivo* kinetics of protein targeting to the endoplasmic reticulum determined by site-specific phosphorylation. *EMBO J* **19**, 6704–6712.
20 Ota K, Sakaguchi M, von Heijne G, Hamasaki N & Mihara K (1998) Forced transmembrane orientation of hydrophilic polypeptide segments in multispanning membrane proteins. *Mol Cell* **2**, 495–503.
21 von Heijne G (1986) The distribution of positively charged residues in bacterial inner membrane proteins correlates with the trans-membrane topology. *EMBO J* **5**, 3021–3027.

22 Mothes W, Heinrich S, Graf R., Nilsson I, von Heijne G, Brunner J & Rapoport T (1997) Molecular mechanisms of membrane protein integration into the endoplasmic reticulum. *Cell* **89**, 523–533.
23 Heinrich S, Mothes W, Brunner J & Rapoport T (2000) The Sec61p complex mediates the integration of a membrane protein by allowing lipid partitioning of the transmembrane domain. *Cell* **102**, 233–244.
24 McCormick PJ, Miao Y, Shao Y, Lin J & Johnson AE (2003) Cotranslational protein integration into the ER membrane Is mediated by the binding of nascent chains to translocon proteins. *Mol Cell* **12**, 329–341.
25 Wahlberg JM & Spiess M (1997) Multiple determinants direct the orientation of signal-anchor proteins: the topogenic role of the hydrophobic signal domain. *J Cell Biol*. **137**, 555–562.
26 Kozak M (1999) Initiation of translation in prokaryotes and eukaryotes. *Gene* **234**, 187–208.
27 Kunkel TA (1987) Rapid and efficient site-specific mutagenesis without phenotypic selection. *Methods Enzymol* **154**, 367–382.
28 Geisselsoder J, Witney F & Yuckenberg P (1987) Efficient site-directed *in vitro* mutagenesis. *Biotechniques* **5**, 786–791.
29 Liljeström P & Garoff H (1991) Internally located cleavable signal sequences direct the formation of Semliki Forest virus membrane proteins from a polyprotein precursor. *J Virol* **65**, 147–154.